

A Molecular Dynamics Simulation Study of the Self-Diffusion Coefficient and Viscosity of the Lennard–Jones Fluid¹

K. Meier,² A. Laesecke,³ and S. Kabelac^{2,4}

Self-diffusion coefficients and viscosities for the Lennard–Jones fluid were obtained from extensive equilibrium molecular dynamics simulations using the Einstein plot method. Over 300 simulated state points cover the entire fluid region from the low-density gas to the compressed liquid close to the melting line in the temperature range $T^* = Tk/\varepsilon = 0.7$ to 6.0. The translational–translational, translational–configurational, and configurational–configurational contributions to the viscosity are resolved over this broad range of fluid states, thus providing coherent insight into the nature of this transport property. The uncertainties of the simulation data are conservatively estimated to be 0.5% for self-diffusion coefficients and 2% for viscosities in the liquid region, increasing to 15% at low-density gaseous states.

KEY WORDS: Einstein relation; equilibrium molecular dynamics; Lennard–Jones fluid; self-diffusion coefficient; transport properties; viscosity; viscosity contributions.

1. INTRODUCTION

The Lennard–Jones potential serves as an important reference model in many applications of statistical mechanics. Furthermore, it is often used to

¹ Paper presented at the Fourteenth Symposium on Thermophysical Properties, June 25–30, 2000, Boulder, Colorado, U.S.A.

² Institut für Thermodynamik, Universität Hannover, Callinstr. 36, D-30167 Hannover, Germany.

³ Physical and Chemical Properties Division, National Institute of Standards and Technology, 325 Broadway, Boulder, Colorado 80303, U.S.A.

⁴ To whom correspondence should be addressed.

predict thermophysical properties of simple fluids or as a building block for intermolecular potential models of complex molecules. The knowledge of its macroscopic thermophysical properties forms an essential basis for these applications. Thermodynamic property surfaces, such as p - ρ - T or u - ρ - T relationships, are now well characterized and can be readily calculated from the latest and most accurate fundamental equation of state for the Lennard-Jones fluid developed by Mecke et al. [1]. However, the transport properties, self-diffusion coefficient, viscosity, thermal conductivity, and bulk viscosity are less well understood. In previous studies, e.g., Refs. 2-8, the uncertainties of simulation data were still up to two orders of magnitude higher than those commonly achieved in experiments.

This paper focuses on the self-diffusion coefficient and viscosity of Lennard-Jones fluid. One objective of this study is to explore both transport properties at near-experimental uncertainty levels. Furthermore, the subdivision of viscosity into translational-translational, translational-configurational, and configurational-configurational contributions which arises naturally in the time correlation function formalism is investigated over a broad range of fluid states.

2. SIMULATION METHODOLOGY

Two approaches exist to simulate transport properties. These are non-equilibrium and equilibrium molecular dynamics [9]. Nonequilibrium simulations provide conceptual problems which make rigorous analysis and interpretation of the results difficult. For example, the artificial removal of heat from a system with thermostating algorithms [10], extrapolation of simulation results to thermodynamic equilibrium [11], and introduction of periodic effects by the commonly employed Lees-Edwards periodic boundary conditions [12] are still under discussion. For these reasons, the equilibrium molecular dynamics method was chosen in this work. Additionally, it allows calculation of the four transport properties, self-diffusion coefficient D , viscosity η , thermal conductivity λ , and bulk viscosity η_b , from a single simulation at one state point.

From equilibrium molecular dynamics simulations, transport properties can be evaluated by two different, but formally equivalent methods. In the Green-Kubo integral method, the transport coefficients are obtained as integrals under time correlation functions of the relevant thermodynamic fluxes [9]. Alternatively, in the Einstein plot method, they are evaluated as the long-time limit of the slope of the mean-squared displacement corresponding to the transport property under investigation [13].

Here, the Einstein relations were chosen over the Green-Kubo integral formulas because the analysis procedure was found to be easier.

The Einstein relations are expressed as

$$D = \lim_{t \rightarrow \infty} \frac{1}{6N} \frac{d}{dt} \left\langle \sum_{\alpha=1}^3 \sum_{i=1}^N [r_{\alpha,i}(t) - r_{\alpha,i}(t_0)]^2 \right\rangle \quad (1)$$

for the self-diffusion coefficient D [9] and

$$\eta = \lim_{t \rightarrow \infty} \frac{V}{6kT} \frac{d}{dt} \left\langle \left[m \sum_{\alpha=1}^2 \sum_{\beta=\alpha+1}^3 \sum_{i=1}^N \{r_{\alpha,i}(t) v_{\beta,i}(t) - r_{\alpha,i}(t_0) v_{\beta,i}(t_0)\} \right]^2 \right\rangle \quad (2)$$

for the viscosity η [13]. N denotes the number of particles, t is the time, V is the volume of the system, T is the thermodynamic temperature, k is Boltzmann's constant, and m is the particle mass. $r_{\alpha,i}$ and $v_{\alpha,i}$ are the Cartesian coordinates and velocity components in the α -direction of particle i . The sum

$$m \sum_{i=1}^N \{r_{\alpha,i}(t) v_{\beta,i}(t) - r_{\alpha,i}(t_0) v_{\beta,i}(t_0)\} = A_{\alpha\beta}(t) - A_{\alpha\beta}(t_0) \quad (3)$$

is proportional to the displacement of the center of β -momentum in the α -direction at time t relative to its position at a time origin t_0 . The sums over α and β take advantage of the fact that the pressure tensor is symmetric for monatomic fluids.

The Einstein relation for viscosity cannot be used directly [5, 14], because it implicitly assumes continuous particle trajectories which are unaffected by boundary effects. Since the trajectories in a finite system simulation with periodic boundary conditions are discontinuous whenever a particle leaves or enters the simulation box, a modification of Eq. (2) is necessary. The difference $A_{\alpha\beta}(t) - A_{\alpha\beta}(t_0)$ in Eq. (3) can be related by simple mathematical manipulations to the time integral of the shear stress

$$A_{\alpha\beta}(t) - A_{\alpha\beta}(t_0) = \int_{t_0}^t \tau_{\alpha\beta}(t) dt \quad (4)$$

between time t and a time origin t_0 [13]. The shear stress itself is given by [9]

$$\tau_{\alpha\beta} = \frac{1}{V} \left(\sum_{i=1}^N m v_{\alpha,i} v_{\beta,i} + \sum_{i=1}^{N-1} \sum_{j=i+1}^N r_{\alpha,ij} F_{\beta,ij} \right) \quad (5)$$

where $F_{\beta, ij}$ is the force in the β -direction with which particle i acts upon particle j . If periodic boundary conditions and the minimum-image convention are employed in a simulation, the time evolution of the shear stresses is, in fact, continuous. Therefore, Eq. (4) provides an indirect way to calculate the viscosity Einstein plots. A more detailed discussion of this issue was given by Erpenbeck in Ref. 15.

In this formalism the viscosity can be divided into three contributions. Equation (5) shows that the shear stress consists of two contributions, a translational contribution depending on the particle velocities only, and a configurational contribution

$$\tau_{\text{tra}, \alpha\beta} = \frac{1}{V} \sum_{i=1}^N m v_{\alpha, i} v_{\beta, i} \quad (6)$$

depending on the particle velocities only, and a configurational contribution

$$\tau_{\text{con}, \alpha\beta} = \frac{1}{V} \sum_{i=1}^{N-1} \sum_{j=i+1}^N r_{\alpha, ij} F_{\beta, ij} \quad (7)$$

depending on the particle positions only. If this subdivision of the shear stress is inserted into Eqs. (2) and (4) and the brackets are multiplied out, three contributions, a translational–translational (tra–tra), a translational–configurational (tra–con), and a configurational–configurational (con–con) contribution to the viscosity are found. Hence, the viscosity can be written as the sum of three contributions:

$$\eta(\rho, T) = \eta_{\text{tt}}(\rho, T) + \eta_{\text{tc}}(\rho, T) + \eta_{\text{cc}}(\rho, T) \quad (8)$$

In contrast to thermodynamic properties of monatomic fluids, such as pressure or isochoric heat capacity, the viscosity cannot be divided into pure translational and configurational parts, but also contains a cross contribution $\eta_{\text{tc}}(\rho, T)$, depending on both particle coordinates and velocities. These three contributions fulfill the limiting cases

$$\lim_{\rho \rightarrow 0} \eta_{\text{tt}}(\rho, T) = \eta_0(T), \quad \lim_{\rho \rightarrow 0} \eta_{\text{tc}}(\rho, T) = 0, \quad \lim_{\rho \rightarrow 0} \eta_{\text{cc}}(\rho, T) = 0 \quad (9)$$

as the density approaches zero, in which $\eta_0(T)$ is the zero-density viscosity obtained from the Chapman–Enskog solution to the Boltzmann equation [16].

3. SIMULATION PROCEDURE

3.1. Simulation Details

For the remainder of this paper, reduced quantities denoted by a superscript asterisk (*) are used [9, 14]. Equilibrium molecular dynamics simulations were performed along 15 isotherms. All simulations were

carried out in the classical molecular dynamics ensemble at constant $NVE\mathbf{P}$, where E stands for the internal energy and \mathbf{P} for the total momentum vector of the system. Input internal energies for a given temperature $T^* = T/k\varepsilon$ and density $\rho^* = N\sigma^3/V$ were calculated from the fundamental equation of state by Mecke et al. [1]. All simulations were performed with 1372 particles. The equations of motion were integrated with the velocity-Verlet method [9] using a time step of $\Delta t^* = \sqrt{\varepsilon/m\sigma^2} \Delta t = 0.003$. After an equilibration period of up to 300,000 time steps, the actual simulations proceeded over 1.5 to 2 million time steps. The cutoff radius $r_C^* = r_C/\sigma$ depended on the density of the state point. It was set to $r_C^* = 5.0$ for $\rho^* > 1.0$, 5.5 for $0.6 < \rho^* \leq 1.0$, and 6.5 for $\rho^* \leq 0.6$. The usual periodic boundary conditions and minimum image convention were applied [9]. Our computer programs are based on FORTRAN listings provided on microfiche as attachments to the book by Allen and Tildesley [9].

The distribution of the simulated state points in relation to the phase boundaries is given in Fig. 1. The simulations extend over a wide range of the fluid region of the phase diagram from the low-density gas to the compressed liquid close to the melting line. The 15 isotherms cover the temperature range between $T^* = 0.7$ to 6.0. Metastable superheated vapor and subcooled liquid states were also included. However, state points which apparently lie in the unstable region were not considered. Unstable states were identified by inspection of simulated heat capacities and isentropic compressibilities. If these thermodynamic properties showed unphysical

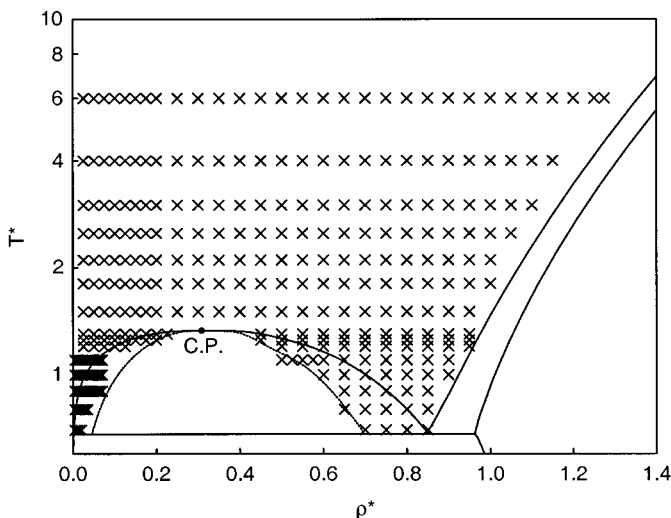


Fig. 1. Distribution of simulated state points in the T^*, ρ^* -plane.

behavior or values, e.g., either negative or very large positive values, a state point was considered to lie in the unstable region.

3.2. Einstein Plot Analysis

The Einstein plots were calculated using separate analysis programs. Diffusion Einstein plots were obtained from the infinite-checkerboard form of the particle trajectories [15], while the mean-squared displacement for the viscosity Einstein plots was calculated according to Eq. (4) by numerical integration of the shear stresses using Simpson's rule.

The slope of the Einstein plots was obtained from a least-squares fit of a straight line to the plot. The interval for the fit was chosen individually for the diffusion plots and the plots for the three viscosity contributions for each simulation. By optical inspection of the plot, it was ensured that the initial behavior was discarded and the fit was done to that part of the plot where the straight line was evident.

4. SELF-DIFFUSION COEFFICIENT

The results for the self-diffusion coefficient are best discussed in terms of the product $D^*\rho^*$, since the self-diffusion coefficient itself tends to infinity as the density approaches zero. However, the product $D^*\rho^*$ remains finite and approaches the dilute gas Chapman-Enskog values in this limit. In Fig. 2 the simulation results for the product $D^*\rho^*$ are given for two selected isotherms, the subcritical isotherm $T^* = 1.2$ and the supercritical isotherm $T^* = 3.0$. Also included are literature data [2, 3, 7, 8] and the correlation by Rowley and Painter [8]. Our data appear to be very consistent and extrapolate well into the zero-density limit. On the isotherm $T^* = 1.2$ a shallow minimum at the approximate reduced density $\rho^* = 0.1$ is observed in the gas region. The isotherm $T^* = 3.0$, however, does not show such a minimum. The data of Rowley and Painter also give a consistent picture but are systematically lower than our data in the liquid region. Since their simulations were performed with 256 particles and ours with 1372 particles, these systematic deviations may be due to finite size effects. On the isotherm $T^* = 3.0$, the literature data sets of Straub [7] and Michels and Trappeniers [2, 3] scatter more than our data. In the gas region the Michels and Trappeniers data lie below our data. As their simulations were carried out with 108 and 125 particles, these systematic deviations may also be attributed to finite size effects. The correlation of Rowley and Painter follows their data well at high densities but fails to describe the correct physical behavior in the gas region.

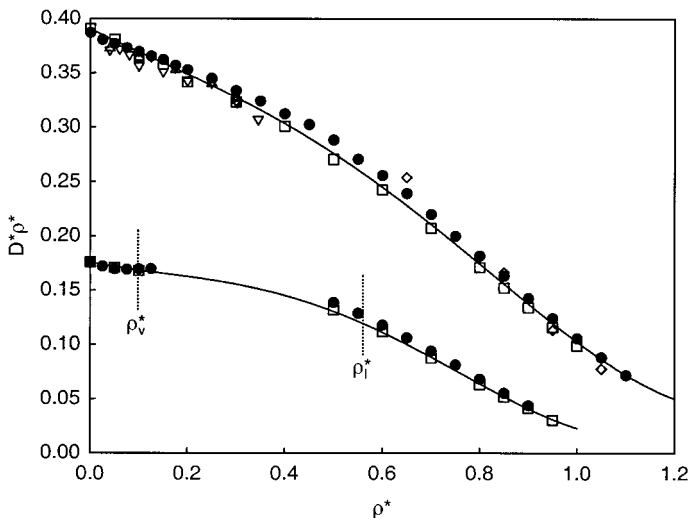


Fig. 2. Product of reduced self-diffusion coefficient and reduced density $D^*\rho^*$ on the subcritical isotherm $T^*=1.2$ and the supercritical isotherm $T^*=3.0$ as a function of reduced density: (●) this work; (Δ) Michels and Trappeniers [2]; (▽) Michels and Trappeniers [3]; (◇) Straub [7]; (□) Rowley and Painter [8]; (—) Rowley and Painter (correlation) [8].

Figure 3 displays the product $D^*\rho^*$ for all 15 simulated isotherms. It characterizes the behavior of the self-diffusion coefficient over the entire fluid region from the triple point up to the reduced temperature $T^*=6.0$. The subcritical isotherms between $T^*=1.0$ and 1.3 also exhibit shallow minima in the gas region, suggesting that the minima are real physical effects. On supercritical isotherms the minima vanish, so that the product $D^*\rho^*$ decreases monotonically with density. The uncertainty of the diffusion data is estimated to be 0.5%. These results demonstrate that molecular dynamics is a useful tool to explore this transport property, which is difficult to access experimentally.

5. VISCOSITY

Figures 4 and 5 show the results for the reduced viscosity and its three contributions for the same selected isotherms $T^*=1.2$ and $T^*=3.0$ which were discussed in Section 4 for the self-diffusion coefficient. Generally, the viscosity data are not as accurate as the self-diffusion data. The uncertainty of our data in the liquid region is estimated to be 2%. However, with decreasing density the scatter of the data becomes larger, reaching 15% at the lowest densities in the gas region.

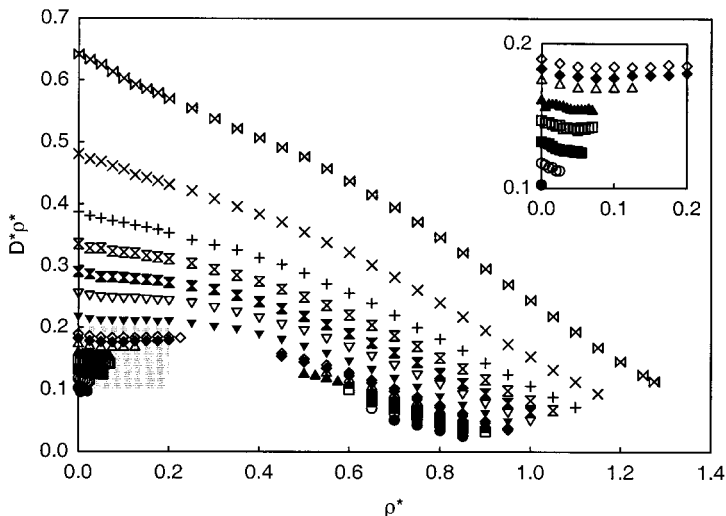


Fig. 3. Product of reduced self-diffusion coefficient and reduced density $D^*\rho^*$ as a function of reduced density ρ^* and reduced temperature T^* : (\circ) $T^*=0.7$; (\bullet) $T^*=0.8$; (\square) $T^*=0.9$; (\blacksquare) $T^*=1.0$; (\blacktriangle) $T^*=1.1$; (\triangle) $T^*=1.2$; (\blacklozenge) $T^*=1.25$; (\diamond) $T^*=1.3$; (\blacktriangledown) $T^*=1.5$; (\triangledown) $T^*=1.8$; (\boxtimes) $T^*=2.1$; (\boxtimes) $T^*=2.5$; (+) $T^*=3.0$; (\times) $T^*=4.0$; (\boxtimes) $T^*=6.0$.

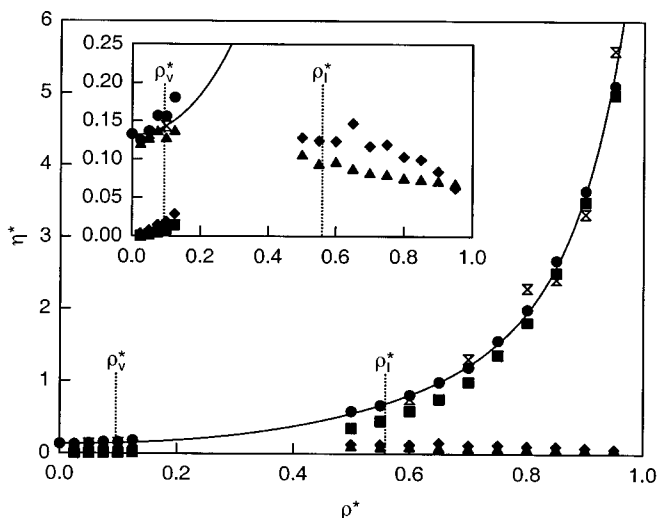


Fig. 4. Reduced viscosity η^* on the subcritical isotherm $T^*=1.2$ as a function of reduced density ρ^* . This work: (\bullet) η^* ; (\blacktriangle) η^*_{it} ; (\blacklozenge) η^*_{ic} ; (\blacksquare) η^*_{cc} . Rowley and Painter [8]: (\boxtimes) η^* ; (—) Correlation.

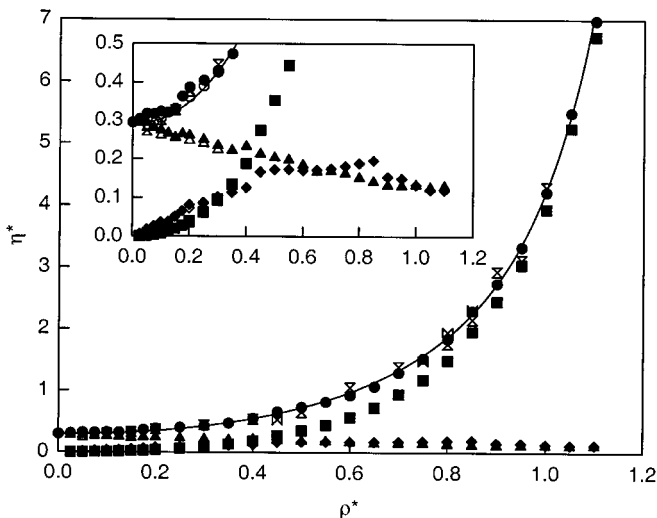


Fig. 5. Reduced viscosity η^* on the supercritical isotherm $T^* = 3.0$ as a function of reduced density ρ^* . This work: (\bullet) η^* ; (\blacktriangle) η_{tt}^* ; (\blacklozenge) η_{tc}^* ; (\blacksquare) η_{cc}^* . Michels and Trappeniers [4]: (\circ) η^* ; (\triangle) η_{tt}^* ; (\diamond) η_{tc}^* ; (\square) η_{cc}^* . Schoen [5]: (\times) η^* . Rowley and Painter [8]: (\boxtimes) η^* . (—) Correlation.

At high densities the viscosity is dominated by the con-con contribution η_{cc}^* , where η_{tt}^* and η_{tc}^* contribute little to the total viscosity. Along an isotherm η_{cc}^* increases exponentially with density. The tra-tra contribution η_{tt}^* yields the largest contribution to the total viscosity at low densities in the gas region and decreases with density. The tra-con contribution η_{tc}^* shows a different behavior. At gaseous densities it increases, reaches a maximum at intermediate densities, and decreases in the high-density region. On the subcritical isotherm $T^* = 1.2$, the maximum is partly covered by the two-phase region. The tra-con contribution η_{tc}^* shows the largest scatter of the three viscosity contributions and appears to be the most difficult to simulate accurately. At liquid densities, our viscosity data show less scatter than the data of Schoen [5] and of Rowley and Painter [8]. Michels and Trappeniers [4] investigated the behavior of the three viscosity contributions on supercritical isotherms up to the reduced density $\rho^* = 0.3$. On the isotherm $T^* = 3.0$, their data are more consistent and systematically lower than our data. However, they used different simulation parameters: a cutoff radius of $r_C^* = 2.5$, 108 particles, and longer simulations, up to 12 million time steps with a length $\Delta t = 0.004$. The systematic deviations are due to the tra-tra contribution, which yields the largest contribution to the total viscosity. The correlation of Rowley and Painter [8] follows our data well

at high densities. However, this is surprising, since it was fitted to only their own data. In the gas region, our data lie above the correlation on both isotherms, suggesting that the correlation predicts gas viscosities that are too low.

Figures 6 to 9 give an overview over all 15 simulated isotherms for the total viscosity η^* and the three contributions η_{tt}^* , η_{tc}^* , and η_{cc}^* , respectively. The total viscosity shows the typical behavior observed for real fluids. It increases with temperature in the gas region, while it decreases in the liquid region. The isotherms intersect at a reduced density of about $\rho^* = 0.75$. The tra-cc contribution η_{cc}^* increases with temperature over the whole density range from the low-density gas up to the compressed liquid. Due to larger uncertainties, the tra-con contribution isotherms are not as clearly distinguishable as for the tra-cc contribution. However, two trends can be observed from Fig. 8. This contribution also increases with temperature over the whole density range, with the maximum being shifted to higher densities as the temperature increases. The con-con contribution η_{cc}^* depends only weakly on temperature up to reduced densities of about $\rho^* = 0.7$. From this point, the isotherms split and diverge. The splitting occurs in the same density range where η_{tc}^* isotherms exhibit their maxima.

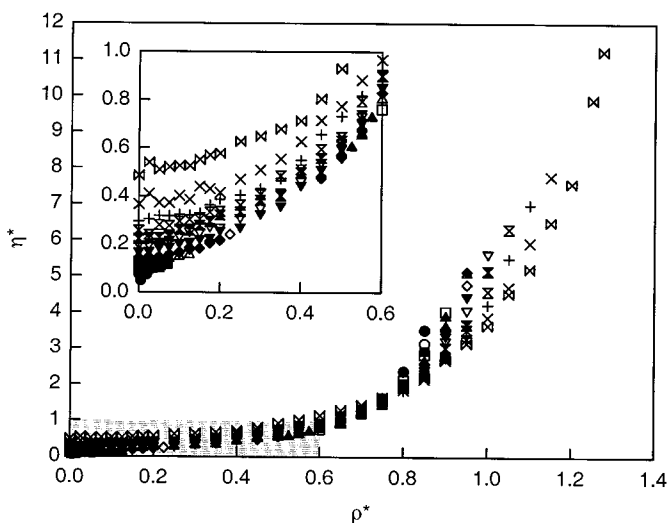


Fig. 6. Reduced total viscosity η^* as a function of reduced density ρ^* and reduced temperature T^* . Symbols the same as in the legend to Fig. 3.

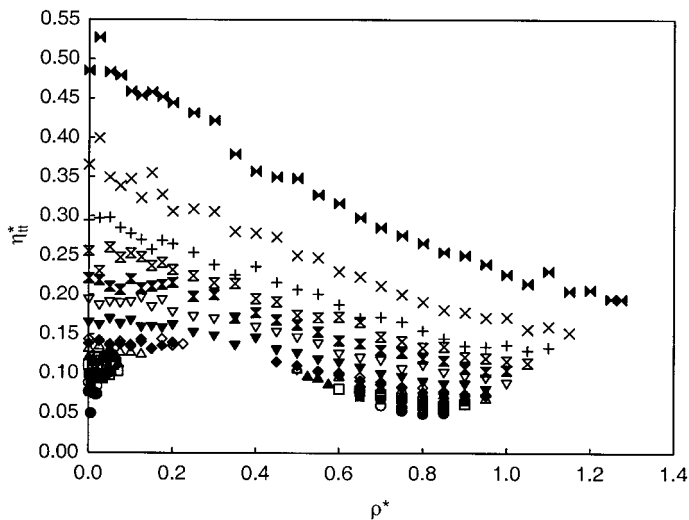


Fig. 7. Reduced translational-translational contribution η_{tt}^* to viscosity as a function of reduced density ρ^* and reduced temperature T^* . Symbols the same as in the legend to Fig. 3.

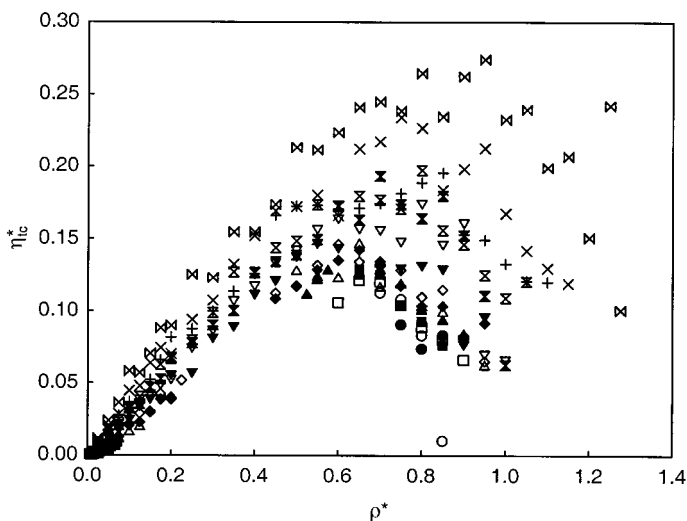


Fig. 8. Reduced translational-configurational contribution η_{tc}^* to viscosity as a function of reduced density ρ^* and reduced temperature T^* . Symbols the same as in the legend to Fig. 3.

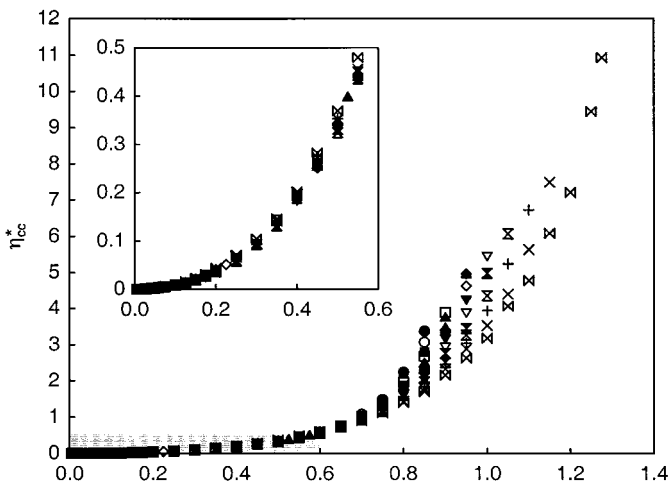


Fig. 9. Reduced configurational–configurational contribution η_{cc}^* to viscosity as a function of reduced density ρ^* and reduced temperature T^* . Symbols the same as in the legend to Fig. 3.

6. CONCLUSIONS

This paper gives an overview of our project to determine the self-diffusion coefficient and viscosity of the Lennard–Jones model fluid with high precision by equilibrium molecular dynamics simulations. By using more particles, larger cutoff radii, and much longer simulations than are considered in conventional simulation work, both transport properties were explored at near-experimental uncertainty levels. The new simulation results for both transport properties are substantially more accurate than in previous studies. The behavior of the three viscosity contributions η_{tt}^* , η_{ic}^* , and η_{cc}^* is characterized over a broad range of fluid states and not only at selected state points. The results of this project will be published in more detail including tabulated simulation data in subsequent papers.

ACKNOWLEDGMENTS

Karsten Meier expresses his gratitude for a guest researcher appointment at the NIST Physical and Chemical Properties Division, Boulder, Colorado. Supercomputing time for this work was provided by the Regionales Rechenzentrum für Niedersachsen (RRZN) at the Universität Hannover, Konrad-Zuse-Zentrum für Informationstechnologie (ZIB) in

Berlin, and NIST Information Technology Laboratory on Cray T3E and SGI Origin parallel computers. Assistance from Dr. Simone Knief (RRZN), Jürgen Fischer (RRZN), and Klaus Ketelsen (Silicon Graphics) in the parallelization and optimization of the MD code is gratefully acknowledged.

REFERENCES

1. M. Mecke, A. Müller, J. Winkelmann, J. Vrabec, J. Fischer, R. Span, and W. Wagner, *Int. J. Thermophys.* **17**:391 (1996).
2. J. P. J. Michels and N. J. Trappeniers, *Chem. Phys. Lett.* **33**:195 (1975).
3. J. P. J. Michels and N. J. Trappeniers, *Physica A* **90**:179 (1978).
4. J. P. J. Michels and N. J. Trappeniers, *Physica A* **133**:281 (1985).
5. M. Schoen, *Berechnung zeitabhängiger kollektiver Eigenschaften von Lennard-Jones Fluiden unter besonderer Berücksichtigung der Scherviskosität*, Dr. rer. nat.-Thesis (Abteilung für Chemie, Ruhr-Universität Bochum, 1987).
6. D. M. Heyes, *Phys. Rev. B* **37**:5677 (1988).
7. J. E. Straub, *Mol. Phys.* **76**:373 (1992).
8. R. L. Rowley and M. M. Painter, *Int. J. Thermophys.* **18**:1109 (1997).
9. M. P. Allen and D. J. Tildesley, *Computer Simulation of Liquids* (Oxford University Press, Oxford, 1987).
10. S. Y. Liem, D. Brown, and J. H. R. Clarke, *Phys. Rev. A* **45**:3706 (1992).
11. K. P. Travis, D. J. Searles, and D. J. Evans, *Mol. Phys.* **95**:195 (1998).
12. J. Petracic and D. J. Evans, *Mol. Phys.* **95**:219 (1998).
13. E. Helfand, *Phys. Rev.* **119**:1 (1960).
14. J. M. Haile, *Molecular Dynamics Simulation—Elementary Methods* (John Wiley, New York, 1992).
15. J. J. Erpenbeck, *Phys. Rev. E* **51**:4296 (1995).
16. J. O. Hirschfelder, C. F. Curtiss, and R. B. Bird, *Molecular Theory of Gases and Liquids* (John Wiley, New York, 1954).